A vinculin tail hotspot mutation in cancer patients affects mouse embryonic fibroblast motility

By
Jasleen Chaddha

Senior Honors Thesis
Department of Biology
University of North Carolina at Chapel Hill

From the Lab of Sharon Campbell
UNC Medical School Department of Biochemistry and Biophysics

Readers:
Adrienne Cox
Zachary Nimchuk

ABSTRACT:

Vinculin, an essential adhesion scaffolding protein, physically links membrane bound integrin and cadherin receptors to filamentous actin. Cells that fail to express vinculin or possess dysfunctional vinculin exhibit rounded morphology, enhanced motility, and resistance to apoptosis and anoikis.[6] Therefore, vinculin is classified as a tumor suppressor protein in which mutations have serious consequences in cancer. A possible 'hotspot' region—an encoded region of a protein that is highly inclined to mutate and phenotypically manifest—has been identified at in the tail-domain of vinculin at residue R925. At this residue, a specific histidine mutation has been linked to several types of cancer. The purpose of this study was to examine the possibility of residue R925 as a hotspot region and test whether the R925H mutation in vinculin enhances motility properties in a model cell line. To examine the status of R925 as a hotspot region, we mined several databases to link certain prevalent mutations in vinculin to different types of cancer. R925H was the most prominent mutation in vinculin that was present in 5 types of cancer, confirming R925 as a hotspot region. In order to assess whether R925H affected the motility of mouse embryonic fibroblasts (MEFs), actin binding and bundling activity of mutant vinculin was compared to that of wild-type vinculin. We found that R925H mutant vinculin had lower actin bundling ability. To evaluate the changes in motility patterns caused by the introduction of R925H, we conducted random motility assays to measure the two-dimensional migration of MEFs on micro-fabricated and microfluidic devices. Mutant MEFs on hydrogels displayed significant differences in motility compared to wild-type cells—particularly in total accumulated distance, persistence and velocity. However, further investigation is required to interpret these findings. The insight on the effects of the R925H mutation on cell motility will serve as one of the first steps to unravel the complexities of vinculin's potential role in several human cancer settings.

INTRODUCTION:

Cytoskeletal proteins have an active role in maintaining cell shape, structure, signaling and mechanical transduction.[1,2] Furthermore, these proteins are fundamental in remodeling the cell in response to environmental stresses.[3] Cytoskeletal remodeling is necessary for a myriad of cellular processes such as cell division, morphology, motility and generation of cellular responses to external mechanical cues.[2,3]

Vinculin is an essential, ubiquitous, and highly conserved scaffolding protein that is involved in anchoring actin to the cell membrane in cell-cell and cell-matrix junctions.[1,4] It is a (~120 kDa) multi-domain protein composed of a large (~90 kD) "head" domain and a smaller (~21 kD) "tail" domain, connected by a proline-rich flexible linker loop (Figure 1).[4] The head and tail interact in an auto-inhibitory fashion that prevents vinculin's scaffold function.[4] The autoinhibitory interactions between these domains are released upon ligand binding and/or post-translational modification.[4] This allows vinculin to interact with various proteins, including actin.[4] Specifically, the head domain of vinculin interacts with cytoskeletal proteins talin, α-catenin, and α-actinin—these interact with integrins and cadherins based junctions, respectively.[1,4] The tail domain binds and bundles actin into large filaments, connecting the cell's cytoskeleton to the extracellular matrix (ECM).[1] Structurally, the vinculin tail domain is composed of five alpha helical bundles, and they interact with paxillin, raver1, and F-actin.[1,4] The tail domain also binds with cell membrane acidic phospholipids, particularly phosphoinositide 4,5-phosphate (PIP2).[1, 4, 5]

Vinculin is localized in cellular adhesions such as focal adhesions and adherens junctions.[4] Focal adhesions form mechanical links between actin bundles within a cell and the ECM. Specifically, these adhesions facilitate interactions involving transmembrane integrins—mechanical proteins that attach the cell cytoskeleton to the ECM.[4] Adherens junctions are

involved in cell-cell adhesion. They occur at cell junctions whose cytoplasmic face is linked to the actin cytoskeleton.[4] At these adhesion sites, vinculin regulates responses to tension forces by mediating the link between transmembrane receptors and actin cytoskeleton.[1,4] Here, vinculin physically links membrane bound integrin and cadherin receptors to filamentous actin.[1] Vinculin is recruited to focal adhesions to regulate cell shape, motility and mechanotransduction.[4] Some of vinculin's roles include the stabilization of adhesions to actin in response to force, the regulation of adhesions at the leading edge of migrating mesenchymal cells, and the mediation of transmission of traction forces.[5] These roles are achieved through vinculin's interactions with over 19 binding partners.[4]

Through its active role in cellular adhesion, vinculin is highly involved in the motility of cells. Cell motility plays an important role at several steps in cancer metastasis, or the spread of cancer cells from the primary tumor to other places in the body.[7] Specific stages of metastasis include escaping the primary tumor, migration to other areas in the body, and movement into distant organs.[7] However, cell lines lacking vinculin have demonstrated phenotypes that share striking similarities with typical cancer cells.[6,7] These phenotypes include a rounded morphology, enhanced cell motility, and resistance to apoptosis and anoikis.[6] Additionally, observations that link the loss of function of vinculin, either through deregulation or mutation, to several types of cancers signify the involvement of vinculin in cancer.[7,8] Consequently, vinculin is classified as a tumor suppressor protein.

A missense histidine mutation in the tail domain of vinculin, in a region important for actin bundling and reorganization and lipid binding, was of particular interest to us. This mutation occurs at the residue of R925 where arginine is mutated to histidine (Figure 1).[4] We examined the possibility of R925 as a 'hotspot' region—an encoded region of a protein that is highly inclined to mutate and phenotypically manifest.[7] Further, we hypothesized that fibroblast

cells expressing R925H mutant vinculin would demonstrate differences in cell motility. Specifically, we sought to examine whether the R925H mutation would render vinculin to malfunction, which would lead to cancer-like cell morphologies and motility. We postulated that mutant fibroblast cells would exhibit higher velocity, lower persistence, and greater accumulated distance. Fibroblasts with dysfunctional vinculin or those that lack vinculin entirely have demonstrated these traits on glass.[6,11,12]

To confirm that the R925 residue is indeed a hotspot region, we conducted a data-mining procedure. Several online cancer genomics databases, such as cBIO portal, COSMIC, and intOGen, were utilized to acquire a collection of vinculin mutations linked to cancer (Supplemental Figure 1). Amongst the 33 mutations found across these databases, one of the most prominent was the R925H mutation in vinculin (Figure 1, Supplemental Figure 1). Linked to a total of 12 cases of cancer patients—the highest number of cases reported for a single mutation—this missense mutation is involved in esophageal, uterine, lung, cervical and stomach cancers (Figure 1, Supplemental Figure 1). Since the R925H was unique, this mutation became of special interest and motivated us to study the changes in motility it induced.

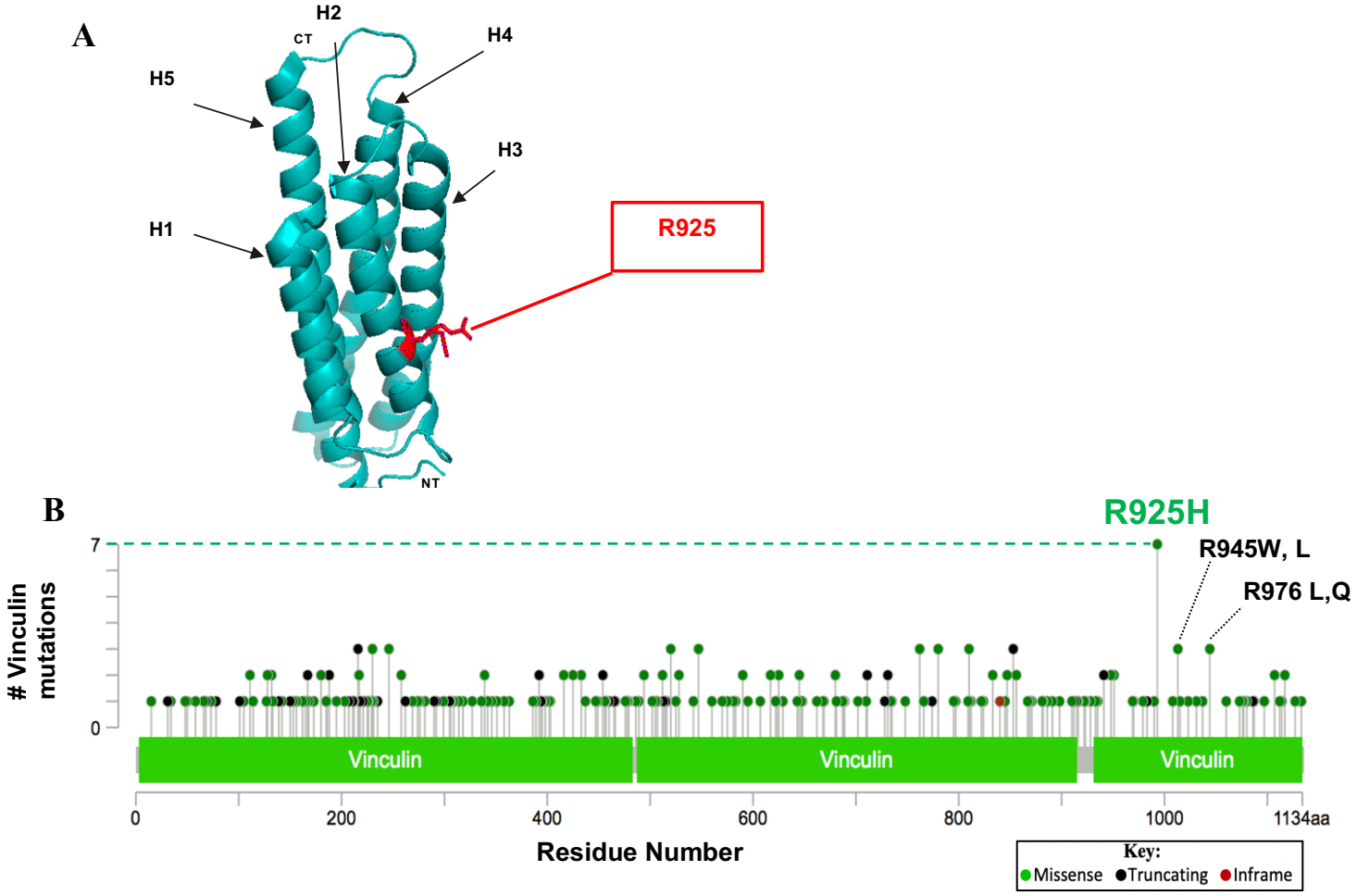

C

Database	Number of Cases Reported	Type of Cancer	Type of Mutation	Position on Vinculin
cBio Portal	7	Esophageal, Uterine, Lung, Cervical	Missense	R925H
cBio Portal	3	Stomach, Cutaneous	Missense	R945W/R945L
cBio Portal	3	Cutaneous, Thyroid, Colorectal	Missense	R976L/R976Q
GDC	5	Esophagus, Stomach, Uterus, Cervix, Lung	Missense	R925H

Figure 1. ***The R925 residue is a hotspot region in the vinculin tail domain and the R925H mutation is linked to 5 types of cancer.*** (**A**) The helical structure of vinculin tail domain is depicted by the turquoise color. The red area highlights the R925 residue where the histidine mutation occurs. This mutation lies in helix 2 of the tail domain. (**B**) In the cBIO Portal, the R925H mutation is implicated in 7 cases of cancer patients. In the data mining worksheet, this mutation was implicated in a total of 12 cases (adapted from *cBIO Portal*). This figure correlates to Supplemental Figure 1. (**C**) This table demonstrates the mutations in the vinculin tail domain that are linked to the highest numbers of cases of cancer (as seen in 1B). The table also lists the types of cancer the mutations are linked to. This table was compiled from *Genomic Data Commons Data Portal (GDC)* and *cBIO Portal.* This table is a truncated version of the data-mining worksheet, see Supplemental Figure 1.

In order to understand whether the mutation affects the motility of cells, first we decided to investigate if R925H mutant vinculin would demonstrate different actin binding and bundling activity as compared to optimally functioning, wild-type vinculin. Actin binding and bundling activity is an essential aspect of cell motility, and in turn mechanotransduction. [1,4] High-speed actin co-sedimentation assays were performed in order to measure the actin binding capabilities of mutant vinculin, wild-type vinculin, and wild-type metavinculin. We conducted low-speed actin co-sedimentation assays to evaluate the actin bundling capabilities of these three proteins as well. Metavinculin is a splice variant of vinculin that is co-expressed with vinculin.[1] This protein contains a 68-residue insertion in the vinculin tail domain that confers lower bundling activities than vinculin.[1,4] Having characterized the binding and bundling properties of metavinculin in depth, we included it in the characterization of actin binding and bundling activity as a control to ensure that the protein purification and actin co-sedimentation assays were being performed correctly.

Random migration assays were implemented to study the differences in motility caused by R925H mutant vinculin. Our experimental design was focused on elucidating the motility of live cells by employing micro-fabrication techniques—particularly, studying fibroblast cells in both liquid media on glass and durotaxis using hydrogels. Durotaxis is a form of cellular migration in which cells are guided by stiffness gradients or cues.[12] Studying durotaxis on hydrogels is beneficial because directional migration across the stiffness gradient in a hydrogel increases mechanic force stimulation on cells. Any mechanical stimulus placed onto cells causes talin to bind to the head domain of vinculin and F-actin to bind to the tail domain. Vinculin then mediates the transmission of traction forces to the rest of the focal adhesion.[1,4] Through the function of many proteins, such as integrin, focal adhesions form mechanical links between intracellular actin bundles and the extracellular environment.[4] Cell membranes then stiffen in

response. The greater mechanical stimulus placed on cells by the stiffness gradient of a hydrogel causes the cell membrane to further stiffen. Increased stiffness in cell membranes are characteristic of tumor cells. [2,6] Stiffness properties of hydrogels can be tuned to better mimic physiological conditions, allowing us to more accurately observe the motility of transformed cells.[6] We used mid-stiffness hydrogels to provide a mechanical stimulus that reasonably approximates the in vivo environment of cancer cells. [6] These physiological conditions are not taken into account when studying motility on glass.

Wild-type vinculin and R925H mutant vinculin were both stably expressed in a mouse embryonic fibroblast (MEF) cell line. The exogenous expression of mutant vinculin in MEFs was equivalent to the endogenous high expression levels of wild-type vinculin in MEFs. MEFs were studied on both glass and mid-stiffness hydrogels. Using MEFs facilitated a clear comparison between the motility results of null, wild-type and mutated cells. We chose this particular cell model system because vinculin knockout MEFs have been well characterized. [6,9,11] Specifically, we have previously studied the morphology, cell migration and mechanotransduction in vinculin knock out MEFs.[6] After conducting the random migration assays and manually tracking each cell, we focused on the specific migration parameters of velocity, accumulated distance and persistence. Velocity of the cell is defined as the speed of a cell's movement. Persistence is the tendency of a cell to move in one particular direction. The accumulated distance is the total amount of distance the cells travel. These properties are thought to be distinctive in cancer cells, which are known to spread uncontrollably across the body, with higher velocity, lower persistence and greater accumulated distance.[6,7,10,12]

This research project begins to unravel the complexities of vinculin's role in cancer initiation or maintenance, and assesses whether the R925H mutation promotes cancerous properties in cells. In addition to determining whether this mutation occurs in a hotspot region,

we were interested in investigating the differences in motility that the vinculin R925H mutation induces. We utilized data-mining procedures, actin co-sedimentation assays and random migration assays to further this investigation. Though R925 was confirmed to be a hotspot region and R925H was found to affect the actin bundling activity of vinculin, only mutant MEFs studied on mid-stiffness hydrogels displayed significant differences in accumulated distance, velocity and persistence.

METHODS:

Cell Culture, DNA Constructs and Generation of Stable Cell Lines:

WT MEFs and vinculin null MEFs were generously supplied by Dr. Brent Hoffman of Duke University. All the cells were cultured in Dulbecco's modified Eagle's medium, DMEM (Invitrogen). The cells were supplemented with 10% fetal bovine serum (Sigma) and penicillin-streptomycin solution (Sigma). The cell cultures were grown with 5% CO_2 in a 37°C incubator.[6]

Dr. Mohammed Ashhar Khan of the Campbell Lab at UNC Chapel Hill generated both wild type and R925H mutant vinculin, which were stably expressed in MEFs. The full-length human vinculin construct (1-1066) was subcloned into the pBabe-puro vector. The constructs were inserted using NgoMIV and SnaBI restriction sites. The pBabe vector was first co-transfected into HEK 293T packaging cell line with pCL-10A1 (15 mg) packaging DNA. Then the media was collected containing the retroviruses. This pBabe retroviral system was utilized to generate stable cell lines.[6] After 48 hours, the viruses were harvested and then used to infect the vinculin null MEFs with polybrene (8 mg/mL) for 24-48 hours. Cells expressing vinculin were selected with puromycin (7.5 mg/mL). The cells were then kept under selection pressure (5 mg/mL puromycin) for about 3 weeks, and sorted for expression by flow cytometry (Supplemental Figure 2). Vinculin expression levels were later confirmed by a Western blot, demonstrating that exogenous expression of mutant vinculin in MEFs is equivalent to the endogenous high expression levels of wild-type vinculin in MEFs.[6] These cells were grown in the same fashion as the null and wild-type MEFs.

Once cell cultures reached 70-80% confluence, they were passaged. Trypsin and DMEM media were placed in a warm bath for 10 minutes. In the laminar hood, an aspirator was used to take up media from original plated cells. Each plate was washed with 5 mL of phosphate-buffered saline (PBS, 1M) and then 2 mL trypsin was added to each plate—this lifted the cells

that were adhered to the surface of the plate. These plates were placed in the incubator for 5 minutes. To avoid further cleavage, 2 mL media was added to each plate to neutralize the trypsin. The new plates were labeled and placed in the laminar hood. We added 9 mL of media to each plate. Then 1 mL of solution from the original plate was added to these new plates, creating a 1:10 ratio of the number of cells in the new plate to those in the original plate. These new plates were incubated for two days.

Protein Expression and Purification:

Dr. Mohammad Ashhar Khan performed protein expression and purification. The vinculin tail domain (Vt, residues 879-1066 of the chicken sequence) was cloned into the pOlinkH vector. Metavinculin tail (MVt, residues 879-1134 of the chicken sequence) was cloned into 2HR-T vector. Vt R925H (Vt sequence with the R925H missense mutation) was prepared using appropriate primers (EtonBiosciences, Durham, NC) and the Q5 site-directed mutagenesis kit (NEB Inc, MA). They were verified by DNA sequencing (EtonBiosciences, Durham, NC). All vectors were transformed into Escherichia coli strain BL21(DE3) and grown at 37 °C and an optical density of 0.6–0.8 (600 nm). [13]

Protein expression was initiated by the addition of isopropyl-D-1-thiogalactopyranoside. The cells were grown at 18 overnight and harvested by centrifugation (4.5k rpm, 30 min). Cell pellets from this were suspended in lysis buffer and then lysed by sonication. Soluble fractions, containing the proteins, were separated from particulate fractions by centrifugation (15k rpm, 45 min). Proteins were purified by affinity separation using Ni-NTA-agarose beads (Qiagen). Wash buffer was run through the column before eluting target proteins using an elution buffer. For His-tag removal, the eluted volume was dialyzed into TEV cleavage buffer overnight at 4 °C. All proteins were collected by running the dialyzed/cleaved volumes over Ni-NTA-agarose beads. Size exclusion chromatography by S100 column (GE, Pittsburg, PA) in gel filtration buffer to

obtain the highest purity. Protein stocks were stored at −80 °C.[13] For exact chemical concentrations and buffer formulas, refer to Table 1 (below).

Table 1. Chemical concentrations and buffer formulas used in protein expression/purification. [13]

Buffer/ Chemical Name	Formula
Isopropyl-D-1-thiogalactopyranoside for Vt	0.5 mM
Isopropyl-D-1-thiogalactopyranoside for MVt/MVtp	1 mM
Lysis buffer for Vt	20 mM Tris, 150 mM NaCl, 5 mM imidazole, 2 mM β-mercaptoethanol, pH 7.5
Lysis buffer for MVt	50 mM Tris, 200 mM NaCl, 10 mM imidazole, 2 mM β-mercaptoethanol, pH 8.0
Wash buffer for Vt	20 mM Tris, 150 mM NaCl, 60 mM imidazole, 2 mM β-mercaptoethanol, pH 7.5 for Vt
Wash buffer for MVt	50 mM Tris, 200 mM NaCl, 25 mM imidazole, 2 mM β-mercaptoethanol, pH 8.0 for MVt/MVtp
Elution buffer for Vt	20 mM Tris, 150 mM NaCl, 500 mM imidazole, 2 mM β-mercaptoethanol, pH 7.5
Elution buffer for MVt	50 mM Tris, 200 mM NaCl, 250 mM imidazole, 2 mM β-mercaptoethanol, pH 8.0
TEV cleavage buffer for Vt	20 mM Tris, 150 mM NaCl, 50 mM imidazole, 2 mM β-mercaptoethanol, pH 7.5
TEV cleavage buffer for MVt	50 mM Tris, 200 mM NaCl, 20 mM imidazole, 2 mM β-mercaptoethanol, pH 8.0
Gel filtration buffer	10 mM Tris, 200 mM KCl, 10 mM imidazole, 2.5 mM $MgCl_2$, 1 mM EGTA, 2 mM DTT, pH 7.5

Actin Co-sedimentation Assays:

Dr. Mohammad Ashhar Khan conducted actin co-sedimentation assays with the purified protein obtained from protein expression and purification procedure. High speed co-sedimentation (150,000 RCF for 60 min at 23 °C) was conducted for the actin binding assay. Low speed-cosedimentation (12,000 RCF for 15 min at room temperature) was conducted for the actin bundling assay. For both binding and bundling assays, the supernatant and pellet were separated and resuspended to equal volumes. Volumes were analyzed by 15% SDS-PAGE. Actin-binding properties were calculated by determining the fractions of proteins present in

pellets. Actin-bundling properties were calculating by determining the fractions of actin present in the pellets. Through ImageJ, densitometry analysis was performed to obtain results.

Hydrogel Preparation and Activation:

Two trials in this study utilized medium stiffness photopolymerizable hydrogels, created by Reem Hakeem of the Bear lab at UNC Chapel Hill. These gels were made from a 12% acrylamide and 0.6% bis-acrylamide mixture containing the photoactivatable crosslinker lithium phenyl-2,4,6-trimethyl-benzoylphosphinate (LAP). Gel polymerization was controlled with a Thor Lab 365 nm UV LED oven, in which a 15 mL drop of the hydrogel mixture was illuminated with a 0.35% LAP for 2 minutes and 15 seconds. A medium stiffness gel (~25 kPa elasticity/stiffness) was prepared by covering a slide coated in polymerizable gel mixture with a 3D printed opaque mask and then revealing the mask at controlled, slow pace using a syringe pump. The gels were coated with Fibronectin (10 mg/mL) via sulfo-SANPAH—a chemical cross-linker (25 mg/mL)—under a UV lamp for 30 mins. The resulting hydrogels were 100 microns thick and were refrigerated.

Random Cell Migration Assay:

On Glass: Glass-bottomed culture dishes (MatTek Corp) were coated with 10 μg/ml fibronectin (FN) at 37˚C for 1 hour. 5-15 mL of the cell culture was added to 2 mL of DMEM in a plate using a micropipette. This was done for each group of cells. Then all the plates were placed in the incubator for 2 hours. The metal caps needed to cover each of the samples were sprayed with 70% ethanol and dried in the laminar hood prior to use. They were then placed on each of the samples and labeled. After putting them in place holders in the VivaView machine, the cells were allowed to settle for 30 minutes. Then the cell positions were picked. To better represent the entire population of cells, cells of different sizes, locations, and morphologies were chosen for each group of cells. In one run, 24 different cells were studied per cell group. Cells

were imaged at 37˚C with 5% CO2 with a 20x objective on an Olympus VivaView FL microscope (Hooker Imaging Core at UNC) at 10-minute intervals over 20 hours.

On Hydrogels: The exact procedure described above was followed with the exception of using hydrogels in the place of the glass-bottomed culture dishes.

Analysis: The manual tracking plug-in within ImageJ was used to track each cell's migration. Cells were tracked until they moved out of the frame or divided. The chemotaxis tool on ImageJ was utilized to collect information regarding the velocity, persistence and accumulated distance of each cell. The data collected was analyzed with a multiple-comparisons ANOVA tests (95% CI) on the PRISM software.

FIGURES:

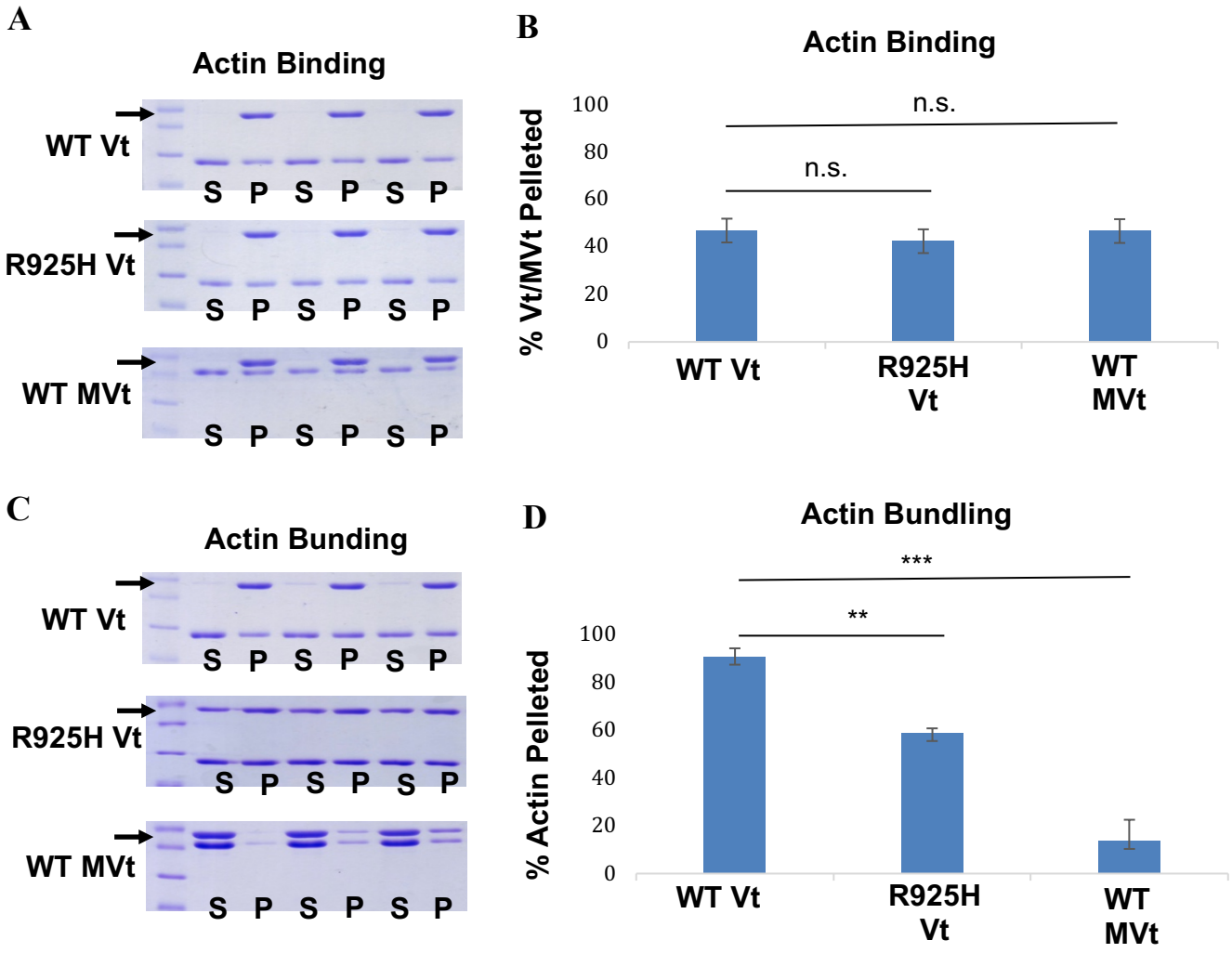

Figure 2. ***R925H mutant vinculin had lower actin bundling ability.*** This data was generated and analyzed by Dr. Mohammad Ashhar Khan. (**A**) SDS-PAGE analysis of high-speed actin co-sedimentation assays completed with wild-type vinculin, R925H mutant vinculin and wild-type metavinculin (S = supernatant, P = pelleted). Arrows indicate lanes representing the amount of vinculin/metavinculin pelleted. (**B**) Quantification of vinculin or metavinculin fractions in pellets represent the actin binding capabilities of wild-type vinculin, R925H mutant vinculin and metavinculin. Error bars represent standard deviation. (**C**) SDS-PAGE analysis of low-speed actin co-sedimentation assays completed with wild-type vinculin, R925H mutant vinculin and wild-type metavinculin (S = supernatant, P = pelleted). Arrows indicate lanes representing the amount of actin pelleted. (**D**) Quantification of actin fractions present in pellets represent the actin bundling capabilities of wild-type vinculin, R925H mutant vinculin and metavinculin. Error bars represent standard deviation. Two-sided t-test indicated by non-significant (n.s.), $p < 0.05$ (*), $p < 0.01$ (**), $p < 0.001$ (***).

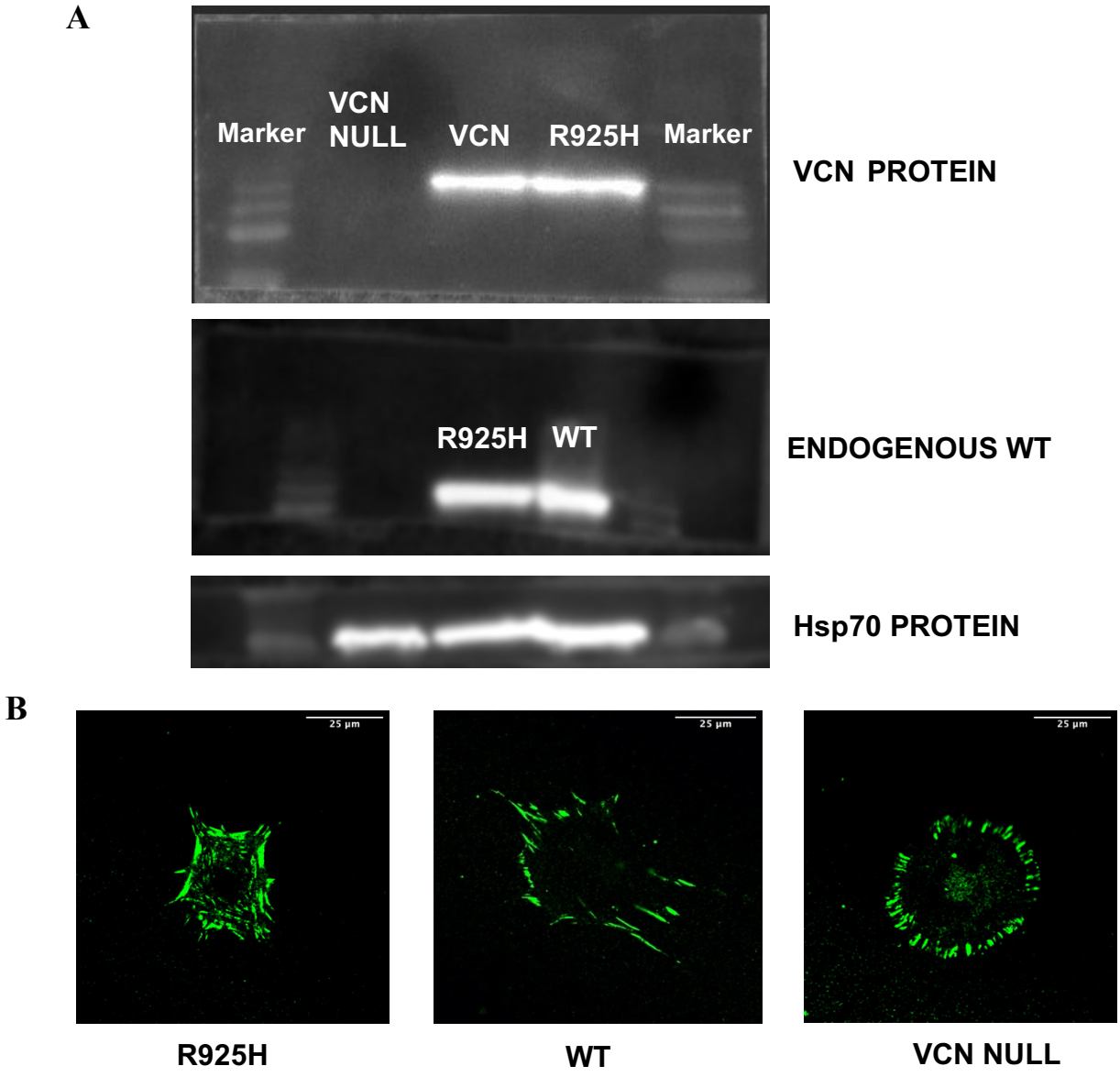

Figure 3. ***Elongated focal adhesions and rounded cell morphology observed in R925H mutant MEFs, which express the same levels of vinculin as wild-type MEFs.*** (**A**) This western blot shows the exogenous expression level of vinculin and R925H vinculin on a vinculin null MEF background. Both expression levels are equivalent to endogenous vinculin expression in WT MEFs. (**B**) Representative fluorescence microscopy images are of the three cell types studied in this experiment. Endogenous vinculin was tagged with mEmerald fluorophore in order to visualize vinculin expression in both mutant R925H MEFs and wild-type MEFs. Vinculin null MEFs were stained for paxillin. The images have a 25 µm scale bar.

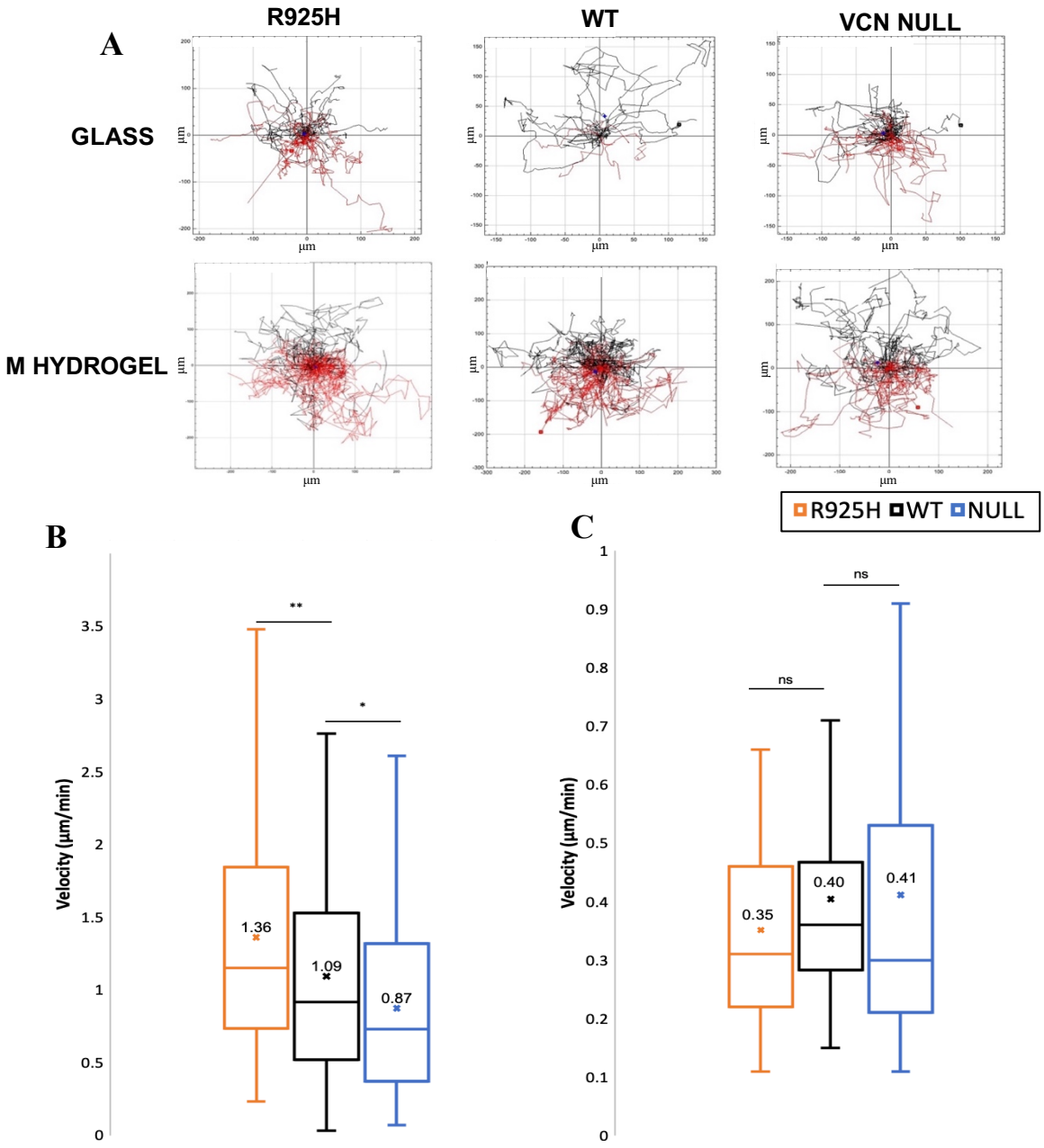

Figure 4. ***R925H mutant MEFs had a higher average velocity on mid-stiffness as compared to wild-type MEFs.*** (**A**)Representative cell tracks plotted for n>20 cells each for wild-type MEFs, vinculin null MEFs, and R925H mutant MEFs on both mid-stiffness hydrogels and glass. Migratory plots were generated using ImageJ. **(B)** In the box and whisker plots, the ends of the box represent upper and lower quartiles (outer 25% velocity values). The box spans the interquartile range (middle 50% velocity values). The horizontal line inside of the box denotes median velocity value. Average velocity is denoted by the X in the box and its value is right above it. This plot shows the velocity of cells on a mid-stiffness hydrogel. A total of 125 R925H mutant MEFs, 184 wild-type MEFs and 104 vinculin null cells were analyzed. **(C)** Box and whisker plots demonstrate the velocity of cells on glass. A total of 85 R925H mutant MEFs, 44 wild-type MEFs and 49 vinculin null cells were analyzed. All significant differences with respect to wild-type MEFs in (**B**) and (**C**) calculated with multiple-comparisons ANOVA tests (95% CI) indicated by non-significant (n.s.), $p < 0.05$ (*), $p < 0.01$ (**), $p < 0.001$ (***).

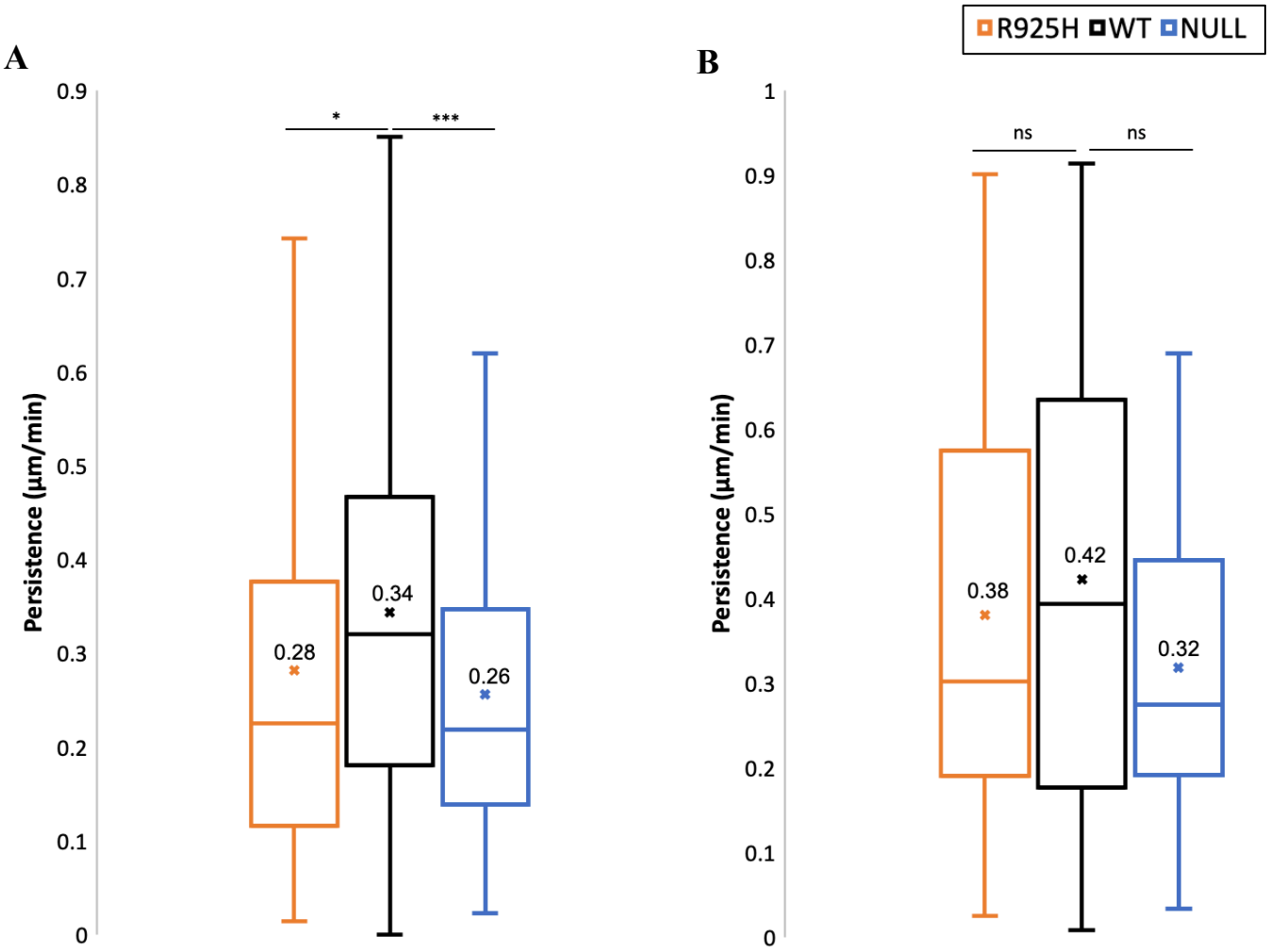

Figure 5. ***R925H mutant MEFs had a lower average persistence on mid-stiffness hydrogel as compared to wild-type MEFs.*** Box and whisker plots can be interpreted in the same fashion as Figure 4. **(A)** Box and whisker plots demonstrate the persistence of cells on a mid-stiffness hydrogel. A total of 125 R925H mutant MEFs, 184 wild-type MEFs and 104 vinculin null cells were analyzed. **(B)** Box and whisker plots demonstrate the persistence of cells on glass. A total of 85 R925H mutant MEFs, 44 wild-type MEFs and 49 vinculin null cells were analyzed. All significant differences with respect to wild-type MEFs in (**A**) and (**B**) calculated with multiple-comparisons ANOVA tests (95% CI) indicated by non-significant (n.s.), $p < 0.05$ (*), $p < 0.01$ (**), $p < 0.001$ (***).

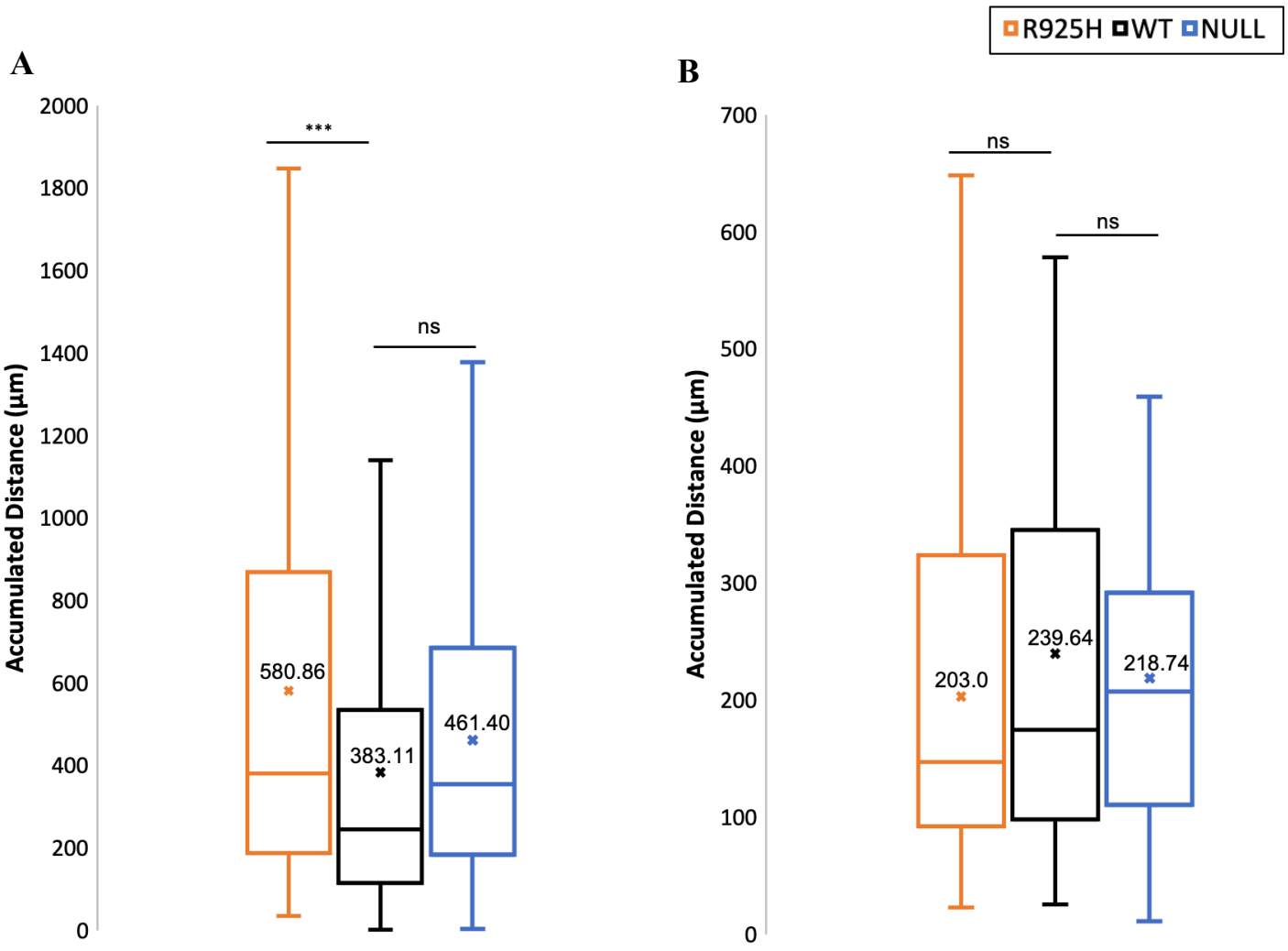

Figure 6. ***R925H mutant MEFs had a higher average accumulated distance on mid-stiffness hydrogel as compared to wild-type MEFs.*** Box and whisker plots can be interpreted in the same fashion as Figure 4. **(A)** Box and whisker plots demonstrate the accumulated distance of cells on a mid-stiffness hydrogel. A total of 125 R925H mutant MEFs, 184 wild-type MEFs and 104 vinculin null cells were analyzed. **(B)** Box and whisker plots demonstrate the accumulated distance of cells on glass. A total of 85 R925H mutant MEFs, 44 wild-type MEFs and 49 vinculin null cells were analyzed. All significant differences with respect to wild-type MEFs in (**A**) and (**B**) calculated with multiple-comparisons ANOVA tests (95% CI) indicated by non-significant (n.s.), $p < 0.05$ (*), $p < 0.01$ (**), $p < 0.001$ (***).

RESULTS:

The R925 residue is a hotspot region in the vinculin tail domain and the R925H mutation is linked to 5 types of cancer.

Vinculin is a scaffolding protein that is localized to focal adhesions, and plays a central role in regulating cell shape, motility and mechanotransduction—properties that are evidently influenced by cancer.[4] Therefore, mutations in vinculin are suspected to induce cancer-like motility.[7] The R925H mutation in the tail domain of vinculin was of interest to us. The first step of this research project was to confirm whether the R925 residue was a hotspot region. In order to do this, we conducted a data-mining procedure to find the links between cancer and mutations in regions encoding the vinculin protein. We probed cancer genomics databases such as cBIO portal, COSMIC, and intOGen. In cBIO portal, 7 cases of cancer—specifically, patients with esophageal, uterine, lung, cervical and stomach cancers—were reported to be linked to the R925H mutation in vinculin (Figure 1). This was the highest number of cancer cases associated with a single missense mutation in the database (Figure 1). After consulting other databases, a total of 33 mutations in vinculin were connected to cases of different types of cancer (Supplemental Figure 1). R925H was implicated in a total of 12 cases of cancer. Again, this was the highest number of cases associated with a single missense mutation. Relative to other residues in vinculin, these data demonstrated that the R925 residue had a higher inclination to mutate and manifest in cancer. This confirmed the R925 residue as a hotspot region and lead us to begin the characterization of the R925H mutation.

R925H mutant vinculin had lower actin bundling ability.

As the R925H mutation was confirmed as a hotspot region, we thought it was important to investigate how this mutation would affect the binding and bundling activity of vinculin (Figure 2). Since the R925H mutation occurred in the vinculin tail domain, a region important in

the process of both binding and bundling actin, we hypothesized that vinculin's ability to bind and bundle actin would be compromised. We conducted high-speed actin co-sedimentation assays to test the binding ability of wild-type vinculin, R925H mutant vinculin and wild-type metavinculin. To test the bundling activity for these three proteins, we conducted low-speed actin co-sedimentation assays. Quantification of the SDS-PAGE analysis of these assays revealed differences among the three proteins in their actin bundling activity. Mutant vinculin exhibited lower actin bundling activity than wild-type vinculin, and this difference was determined to be significantly different ($p < 0.01$) (Figures 2C and 2D). This demonstrated that the R925H mutant vinculin had lower actin bundling activity. However, the difference of actin bundling activity between mutant vinculin and wild-type vinculin was not statistically different—signifying that bundling activities of both proteins were similar (Figures 2A and 2B). Therefore, we concluded that the R925H mutation in vinculin caused a decrease in actin bundling activity as compared to wild-type vinculin.

Elongated focal adhesions and rounded cell morphology observed in R925H mutant MEFs, which express the same levels of vinculin as wild-type MEFs.

Since the R925H mutant vinculin demonstrated lower bundling activity, we further studied how this mutation would manifest in cellular phenotype (Figure 2). We hypothesized that R925H mutant MEFs would demonstrate visual differences in focal adhesions and cell morphology as compared to wild-type MEFs. We chose the MEF model cell line for this experiment because vinculin knockout MEFs have been well characterized in previous studies.[6,9,11] MEFs facilitated a clear comparison between the motility results of null, wild-type and mutant cells. All MEFs were sorted by flow cytometry and quantified by a western blot (Figure 3A, Supplemental Figure 2). Endogenous vinculin expression in both R925H mutant MEFs and wild-type MEFs were determined to be equal (Figure 3A). Vinculin null MEFs

demonstrated little to no vinculin expression. The random motility assays were only conducted with MEFs that expressed high levels of wild-type and mutant vinculin (Supplemental Figure 2). To visualize the differences between mutant, wild-type and null MEFs, fluorescence microscopy images were taken of all three cell types (Figure 3B). Endogenous vinculin tagged with mEmerald fluorophores allowed us to observe the focal adhesions in mutant and wild-type MEFs. Paxillin staining was used to visualize focal adhesions in vinculin null MEFs. R925H mutant MEFs demonstrated larger, elongated focal adhesions. Moreover, mutant MEFs showed a more compact, rounded cell morphology. Whereas, wild-type MEFs demonstrated larger cell shape and smaller focal adhesions. Vinculin null MEFs were completely circular in shape and had the smallest focal adhesions, which corroborated previous characterization of cell morphology of vinculin null MEFs (Figure 3B).[6] In sum, the R925H mutation induced elongated focal adhesions and rounded cell morphology in MEFs.

R925H mutant MEFs had a higher average velocity on mid-stiffness hydrogel as compared to wild-type MEFs.

After studying differences in focal adhesions, we next tested whether specific aspects of migration were affected by the mutation. We hypothesized that the R925H mutant MEFs would demonstrate a higher velocity than wild-type MEFs. To measure the velocity of all three cell types on both hydrogels and glass, individual cell tracks from the random migration assays were manually tracked and velocity values for each cell were generated using the chemotaxis tool on ImageJ (Figure 4A). It is important to note that the average velocity value for wild-type MEFs was used as the standard to which the other cell types were compared to in a multiple-comparisons ANOVA test (95% CI). For the MEFs tracked on mid-stiffness hydrogels, R925H mutant cells showed a higher average velocity than both wild-type and null cells. The R925H mutant, wild-type, and null MEFs had average velocities of 1.36 μm/min, 1.09 μm/min, and 0.87

μm/min, respectively, on hydrogels. The average velocity of mutant MEFs was found to be statistically greater than the average velocity of wild-type MEFs ($p < 0.01$). Vinculin null MEFs demonstrated a significantly lower average velocity than that of wild-type MEFs ($p < 0.05$) (Figure 4B). On the other hand, contrasting results were observed on glass surface—R925H mutant, wild-type, and null MEFs had average velocities of 0.35 μm/min, 0.40 μm/min, and 0.41 μm/min, respectively on glass. The R925H mutant MEFs demonstrated the lowest velocity out of all three cell types. The difference in velocity between wild-type and mutant MEFs was deemed to not be statistically significant—the same was observed for the difference in velocity between wild-type and vinculin null MEFs (Figure 4C). Overall, this data demonstrated that the R925H mutant MEFs demonstrated a higher velocity than wild-type and vinculin null MEFs on the mid-stiffness hydrogel.

Notably, the average velocity of vinculin null MEFs was not determined to be statistically different from wild-type and mutant MEFs. This data is inconsistent with previous data that reports that vinculin null cells statistically demonstrate the highest velocity on glass.[6,9] The variance between our data and literature values could be attributed to the difference between experimental conditions utilized for motility assays conducted on glass. Differences include incubation period, magnification, tracking time interval, and the number of cells analyzed.[6] Due to this contradiction, we cannot conclude that mutant MEFs have a higher velocity than wild-type or null MEFs. Rather, we conclude that the R925H mutation causes a possible difference in velocity. To elucidate precise differences in velocity caused by this mutation, further investigation is required.

R925H mutant MEFs had a lower average persistence on mid-stiffness hydrogel as compared to wild-type MEFs.

To study other specific aspects of migration that were affected by the R925H mutation, we also explored the differences in persistence observed across the three cell types on both mid-stiffness hydrogels and glass. Persistence is defined as the tendency of the cell to move in one particular direction. We hypothesized that R925H mutant MEFs would demonstrate less persistence than wild-type MEFs. The values of persistence for each type of MEF were obtained in the same manner as the velocity values were. Average persistence values were compared using multiple-comparisons ANOVA tests (95% CI). On hydrogels, R925H mutant, wild-type and null MEFs demonstrated average persistence values of 0.28 μm/min, 0.34 μm/min, and 0.26 μm/min, respectively. The average persistence of mutant R925H and wild-type MEFs were determined to be statistically different ($p < 0.05$). Additionally, the wild-type MEFs demonstrated a significantly higher average persistence than that of vinculin null MEFs ($p < 0.001$). Average persistence values calculated from random motility done on glass exhibited a similar trend to those done on hydrogels. R925H mutant, wild-type, and null MEFs had average persistence values of 0.38 μm/min, 0.42 μm/min, and 0.32 μm/min, respectively on glass. However, the average persistence of null and mutant MEFs were not deemed to be statistically different from that of wild-type MEFs. All of these data demonstrated that R925H mutant MEFs demonstrated a significantly lower average persistence on mid-stiffness hydrogels. However, we cannot conclude that mutant MEFs have lower persistence than wild-type MEFs because of the insignificant differences observed in persistence values of MEFs analyzed on glass. From this data, we conclude that the R925H mutation causes a possible difference in persistence. Precise conclusions about persistence caused by this mutation requires further research.

R925H mutant MEFs have a higher average accumulated distance on mid-stiffness hydrogel as compared to wild-type MEFs.

The last aspect of migration that we analyzed was accumulated distance, which is defined as the total amount of distance a cell travels. Just as velocity and persistence, accumulated distance was measured in all three cell types, observed on both hydrogels and glass, and compared with a multiple-comparisons ANOVA test (95% CI). We hypothesized that mutant MEFs would demonstrate greater accumulated distance than both null and wild-type cells. Average accumulated distance on hydrogels for mutant, wild-type, and null MEFs were determined to be 580.86 μm, 383.11 μm, and 461.40 μm, respectively. The average accumulated distance of R925H mutant MEFs was determined to be significantly higher than that of wild-type cells ($p < 0.001$). However, the difference between the average accumulated distance between wild-type and null MEFs was not deemed to be statistically different. This trend was not observed on glass—R925H mutant, wild-type, and null MEFs had average accumulated distances of 203.00 μm, 239.64 μm, and 218.74 μm, respectively. These values indicate that the R925H MEFs traveled the least amount of total distance out of the three cell types. Further, the average accumulated distance of null and mutant MEFs were not statistically different from that of wild-type MEFs. Overall, these data demonstrated that R925H mutant MEFs had a significantly higher average accumulated distance on mid-stiffness hydrogels. However, accumulated distance of MEFs studied on glass was determined to not be statistically different among the three cell types. Similarly, to velocity and persistence, further investigation is required to draw precise conclusions regarding accumulated distance. From the data we gathered, we can only conclude that the R925H mutation induces a possible difference in accumulated distance.

DISCUSSION:

Our original hypothesis was that the R925 residue would be a hotspot region and that MEFs expressing the R925H mutation would induce cell morphology similar to those of cancer cells. Further, we speculated that MEFs expressing this mutation would demonstrate actin bundling deficiencies and show differences in cell motility—specifically, higher velocity, lower persistence and greater accumulated distance. These properties would be similar to the motility traits demonstrated by vinculin null MEFs.[6,9,11,12]

The R925H mutation in the tail domain of vinculin was associated with 12 reported cases of cancer, the greatest number of cases involved with one mutation out of the 33 mutations found in cancer databases. This prominent mutation was linked to esophageal, uterine, lung, cervical, and stomach cancers. Our collected data demonstrates that the R925H mutation has a higher propensity to mutate and manifest cancer phenotypes relative to other regions in vinculin. Therefore, R925H was confirmed to occur in a hotspot region. Further, the importance of the R925 residue is emphasized by the critical role it plays in the vinculin tail domain for both actin reorganization and lipid interactions. Our data demonstrates that the R925H mutant vinculin shows lower actin bundling activity. Additionally, this hotspot mutation was observed to cause some differences in the phenotype. Notably, mutant MEFs displayed elongated and more numerous focal adhesions than wild-type MEFs. Mutant MEFs also demonstrated more rounded and compact morphology than the other two cell types.

Random motility assays aimed to differentiate between the motility of MEFs with the R925H mutant MEFs, wild-type MEFs, and vinculin null MEFs. Random motility assays showed that there were insignificant differences between the velocity, persistence, and accumulated distance of wild-type MEFs and mutant MEFs. The MEF cells on mid-stiffness hydrogels, however, demonstrated significant differences between the mutated and wild-type

cells. The mutant MEFs expressed greater velocity, higher accumulated distance, and lower persistence. The differences observed in trends of migratory parameters observed on glass and mid-stiffness hydrogels, along with the data that demonstrated the phenotypic tendencies of MEFs expressing mutant vinculin, allowed us to conclude that the R925H mutant causes changes in motility. Further investigation is required to draw exact interpretations of what aspects of motility are affected in cells expressing the R925H mutation.

R925H mutant vinculin was actin bundling deficient, which correlated to the extensively-characterized LD-CT (vinculin R1060Q/K1061Q) vinculin variant.[14] This variant retained actin binding but showed significant deficiency in F-actin crosslinking, otherwise known as actin bundling. This study concluded that the decrease in actin-bundling was not due to a decrease in the ability of MEFs to respond to external forces, but rather due to a disruption of the ability of vinculin to crosslink actin. Further, this study emphasized that the role of vinculin in mechanotransduction and cell stiffness is primarily driven by actin binding and crosslinking. [14] Paralleling this study, the R925H mutation is also perceived to cause a disruption of the ability of vinculin to crosslink actin. This could affect actin assembly and disassembly at focal adhesions during the migration of the cell.

Nascent focal adhesions are thought to have rapid vinculin activation and turnover, causing faster actin assembly and disassembly. Related to having faster velocity, cells that turn over their focal adhesions quickly can display phenotypes related to a loss of a tumor suppressor, such as promoting metastasis of cancer cells. [14] Focal adhesions in vinculin null cells resemble nascent focal adhesions described.[6,11,12] This led us to predict that the motility of vinculin null cells was representative of the motility of cancer cells. Since the R925H mutation was linked to several types of cancer, we originally postulated that the mutant cells would also demonstrate migratory properties similar to that of vinculin null cells and cancer cells.

However, the motility of the MEF cells studied on glass contradicted the results published in previous literature.[6,9] The R925H mutation is suspected to compromise the functions of vinculin, which in theory would lead to these mutant cells expressing phenotypes similar to those of vinculin null cells—these phenotypic properties are correlated with cancer like metastasis in MEF cells.[11,12] These traits of cell motility involve a higher velocity, less persistence and a greater accumulated distance. However, our results pertaining to glass did not provide significant differences between the velocity, persistence, or accumulated distance. This is of concern because previous literature has claimed that vinculin null cells migrating on glass should exhibit higher speed motility and more migration on glass compared to the wild-type cells, according to previously published studies.[6,9]

The variance among results can partly be attributed to the difference between the experimental conditions used for each of the random motility assays conducted on glass. Previous studies utilized a 24-hour incubation period after plating the cells, while our experiments used a 2-hour incubation period.[6] Further, the previous studies implemented a 10x magnification and a 10-hour tracking time interval.[6] We utilized 20x magnification and a 20-hour tracking time interval. These distinctions in data collection factors could be responsible for the differences observed in the results. Moreover, the number of cells tracked on glass in this experiment was substantially less than the number of cells studied in previous literature.[6] A greater population of cells in each group allowed previous studies to draw statistically significant conclusions. Additionally, since the values for both wild-type and mutant cells for each parameter were very similar, it can be considered that the mutation made little to no difference in the cells' motility—which further negates our original hypothesis.

We expected mutant MEFs studied on mid-stiffness hydrogels to demonstrate similar motility to the vinculin null cells studied in previous literature as well.[6,9] MEFs studied on

hydrogels corroborated our hypothesis because R925H mutants exhibited higher velocity, lower persistence, and more accumulated distance than the wild-type MEFs. These properties of motility could have been induced by the greater mechanical stimulus placed on the MEFs by the mid-stiffness hydrogels. Since greater mechanical stimulus causes migrating cells to have cell membranes with increased stiffness, mid-stiffness hydrogels mimic physiological conditions of cancer cells. This is not taken into account when studying motility on glass.[6] However, there were slight inconsistencies with the vinculin null MEFs on the hydrogels.

One inconsistency observed in the random motility assay conducted on hydrogels was that the difference between average accumulated distance of wild-type and null MEFs was deemed statistically insignificant. Though the mutant cell group demonstrated more accumulated distance than that of the wild-type cells, the null cells did not display an equally high accumulated distance. Additionally, vinculin null MEFs did not demonstrate the expected similar velocity or persistence as those of R925H mutant MEFs. Though further research needs to be conducted on this aspect of MEF cell motility, we conjecture that these inconsistencies could be attributed to cells lacking vinculin and consequently the loss of the scaffold when exposed to the mechanical force of the mid-stiffness hydrogel.

A possible error that could have contributed to the difference between the random motility results of previous literature and those of this experiment on glass is that the media used to grow the cells could have been contaminated. This could affect the morphology of the cells and their ability to grow. Specifically, for the random motility assays conducted on glass, a small amount of debris was observed in the media in a portion of the frames when selecting positions for tracking migration pathways. This could affect the migratory pathways of the cells, which in turn would have affected our results. An improvement that could be made to this experiment is to strengthen the criteria that each cell needs to meet in order to be tracked. In this study, cells were

tracked as long as they stayed within the frame and up until they divided. Perhaps, it is worthwhile to only track cells that do not leave the frame at all in the 60-minute time period and exclude cells that divide from the data. This will rid the experiment of some extraneous factors that could affect the motility of the cells.

Outside of these inconsistencies, it could be extrapolated that there are significantly different cell motility patterns observed between R925H mutants and wild-type MEFs. The R925H mutation does cause a difference in cell motility, though further investigation is required to analyze which aspects of motility are affected. Future directions involving the characterization of the R925H mutation involve repeating random motility assays on mid-stiffness hydrogels with more cells (n>200 per cell type). In addition, we will study motility on low-stiffness and high-stiffness hydrogels. We will also categorize and quantify the focal adhesions in mutant cells. Furthermore, morphological changes induced by this mutation in the cell could be more closely observed, including the effects of the R925H mutation on vinculin's interactions with other proteins. Cell proliferation assays will also be conducted to understand how this mutation affects cell division. Lastly, we could examine the possibility of the R925H mutation upregulating and downregulating other missense mutations in vinculin itself. However, the primary insights on the effects of the R925H mutation on cell motility described by this project will serve as one of the first steps to unravelling vinculin's potential role in inducing cancer-like properties in cells.

ACKNOWLEDGEMENTS:

Firstly, I would like to thank my principal investigator, Dr. Sharon Campbell, for allowing me to have an enriching experience as an undergraduate researcher in her lab. I would also like to thank my research mentor, Dr. Mohammad Ashhar Khan, for providing me opportunities to conduct research, training me in specific laboratory skills relating to this project, and providing valuable guidance in this research project. Thank you to Dr. Muzzadid Sarker for initially training me in the lab. I would also like to thank the rest of Campbell Lab for building a flourishing academic environment for me to learn so much in. I would like to thank the Department of Biophysics and Biochemistry at the UNC Medical School for providing us the opportunity to conduct this study. Thank you to Dr. James E. Bear for giving us the chance to work on this collaborative project. Thank you to Reem Hakeem and Zayna King of Bear Lab for providing thoughtful guidance and assistance throughout the course of this project. Thank you to Dr. Brent Hoffman of Duke University for providing us with wild-type MEFs and vinculin null MEFs. Lastly, I would like to thank Dr. Amy Maddox and the rest of the honors thesis class for their support and helpful feedback.

SUPPLEMENTAL FIGURES

Database	Number of Cases Reported	Type of Cancer	Type of Mutation (Base Change)	Vinculin Position
cBio Portal	7	Esophageal, Uterine, Lung, Cervical	Missense	R925H
cBio Portal	3	Stomach, Cutaneous	Missense	R945W/R945L
cBio Portal	3	Cutaneous, Thyroid, Colorectal	Missense	R976L/R976Q
cBio Portal	2	Prostate	Missense	R1039W
cBio Portal	3	Uveal, Angiosarcoma, Brain	Missense	R785
cBio Portal	3	Colorectal, Pancreatic	Missense	D742N/E
cBio Portal	5	Breast, Colorectal, Skin Cutaneous	Missense	R712H/C/S
cBio Portal	3	Uterine, Cervical, Pancreatic	Missense	R694Q
COSMIC	2	Breast	Missense	I1046T
COSMIC	2	Hematopoietic and Lymphoid	Missense	A1003T
COSMIC	2	Hematopoietic and Lymphoid	Missense	L899V
intOGen	1	N/A	Synonymous variant	AA947
intOGen	1	N/A	Missense	AA963
intOGen	1	N/A	Missense	AA1008
intOGen	1	N/A	Missense	AA1017

intOGen	1	N/A	Synonymous variant	AA1033
intOGen	1	N/A	Missense	AA1044
intOGen	1	N/A	Missense	AA1054
GDC	5	Esophagus, Stomach, Uterus, Cervix, Lung	Missense	R925H
GDC	2	Colon, Rectum	Missense	R1049Q
GDC	2	Corpus Uteri, Uterus	Missense	D880N
GDC	2	Colon, Rectosigmoid junction	Missense	A901V
GDC	2	Corpus Uteri, Uterus	Missense	D788Y
OASIS	1	Colon	Missense	K779R
OASIS	1	Colon	Missense	A833V
OASIS	1	Gastric	Missense	A887T
OASIS	1	Head-Neck	Missense	S944T
OASIS	1	Head-Neck	Missense	A976V
OASIS	1	Lung	Missense	R895L
OASIS	1	Ovarian	Missense	T941N
OASIS	1	Rectal	Missense	R981Q
OASIS	1	Uterine	Missense	R940

Supplemental Figure 1. ***Data mining procedure demonstrates that R925 is a hotspot region.*** Databases used to compile this data: cBIO Portal, Catalogue of Somatic Mutations in Cancer (COSMIC), Integrative Oncogenomics (intOGen), Genomic Data Commons Data Portal (GDC), Atlas of Genetics and Cytogenetics in Oncology and Haematology Data Portal (OASIS).

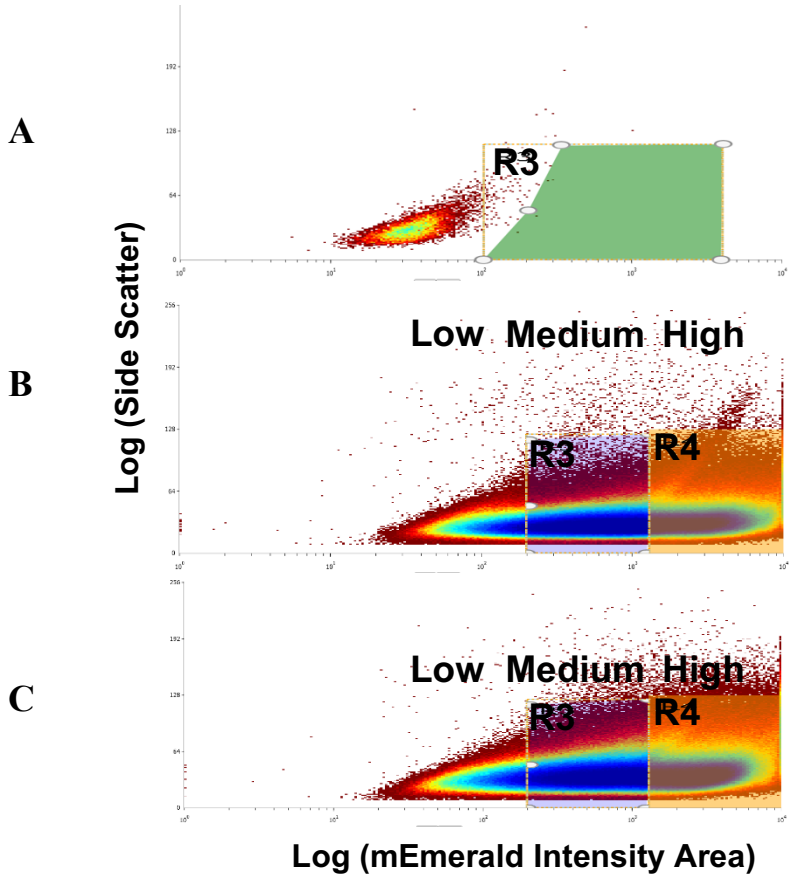

Supplemental Figure 2. ***mEmerald vinculin and mEmerald R925H mutant vinculin were sorted for expression level using flow cytometry.*** Dr. Mohammad Ashhar Khan performed flow cytometry and generated all cell sorting plots in this figure. For all panels, gate R3 represents the proportion of MEFs that had a 'medium' level of vinculin expression and R4 represents the proportion of MEFs that had a 'high' level of vinculin expression. (**A**) Sort data for mEmerald vinculin in vinculin null MEFs. Vinculin null MEFs with the no expression of vinculin were chosen for random motility assays. (**B**) Sort data for mEmerald vinculin in wild-type vinculin MEFs. Wild-type MEFs with high expression of vinculin were chosen for random motility assays. (**C**) Sort data for mEmerald R925H mutant vinculin in wild-type vinculin MEFs. Mutant MEFs with high expression of mutant vinculin were chosen for random motility assays.

REFERENCES:

1.Thompson, P. M., Tolbert, C. E., & Campbell, S. L. (2013). Vinculin and metavinculin: Oligomerization and interactions with F-actin. *FEBS Letters*, *587*(8), 1220–1229.

2. Coll, J. L., Ben-Ze'ev, A., Ezzell, R. M., Rodríguez Fernández, J. L., Baribault, H., Oshima, R. G., & Adamson, E. D. (1995). Targeted disruption of vinculin genes in F9 and embryonic stem cells changes cell morphology, adhesion, and locomotion. Proceedings of the National Academy of Sciences of the United States of America, 92(20), 9161–9165.

3. Spichal, M., & Fabre, E. (2017). The Emerging Role of the Cytoskeleton in Chromosome Dynamics. Frontiers in genetics, 8, 60.

4. Kim, L. Y., Thompson, P. M., Lee, H. T., Pershad, M., Campbell, S. L., & Alushin, G. M. (2016). The Structural Basis of Actin Organization by Vinculin and Metavinculin. *Journal of Molecular Biology*, *428*(1), 10–25.

5. Thompson, P. M., Tolbert, C. E., Shen, K., Kota, P., Palmer, S. M., Plevock, K. M., … Campbell, S. L. (2014). Identification of an Actin Binding Surface on Vinculin that Mediates Mechanical Cell and Focal Adhesion Properties. *Structure*, *22*(5), 697–706.

6. Lee, H. T., Sharek, L., O'Brien, E. T., Urbina, F. L., Gupton, S. L., Superfine, R., … Campbell, S. L. (2019). Vinculin and metavinculin exhibit distinct effects on focal adhesion properties, cell migration, and mechanotransduction. *Plos One*, *14*(9).

7. Tokheim, C. J., Papadopoulos, N., Kinzler, K. W., Vogelstein, B., & Karchin, R. (2016). Evaluating the evaluation of cancer driver genes. Proceedings of the National Academy of Sciences of the United States of America, 113(50), 14330–14335.

8. Subauste, M. C., Pertz, O., Adamson, E. D., Turner, C. E., Junger, S., & Hahn, K. M. (2004). Vinculin modulation of paxillin-FAK interactions regulates ERK to control survival and motility. The Journal of cell biology, 165(3), 371–381.

9. Xu, W., Baribault, H. & Adamson, E. D (1998). Vinculin knockout results in heart and brain defects during embryonic development. Development 125, 327–337.

10. Graham, D. M., Andersen, T., Sharek, L., Uzer, G., Rothenberg, K., Hoffman, B. D., Rubin, J., Balland, M., Bear, J. E., & Burridge, K. (2018). Enucleated cells reveal differential roles of the nucleus in cell migration, polarity, and mechanotransduction. The Journal of cell biology, 217(3), 895–914.

11. Thievessen, I., Thompson, P. M., Berlemont, S., Plevock, K. M., Plotnikov, S. V., Zemljic-Harpf, A., … Waterman, C. M. (2013). Vinculin–actin interaction couples actin retrograde flow to focal adhesions, but is dispensable for focal adhesion growth. *The Journal of Cell Biology*, *202*(1), 163–177.

12. Rothenberg, K. E., Scott, D. W., Christoforou, N., & Hoffman, B. D. (2018). Vinculin Force-Sensitive Dynamics at Focal Adhesions Enable Effective Directed Cell Migration. *Biophysical Journal*, *114*(7), 1680–1694.

13. Sarker, M., Lee, H. T., Mei, L., Krokhotin, A., de Los Reyes, S. E., Yen, L., Costantini, L. M., Griffith, J., Dokholyan, N. V., Alushin, G. M., & Campbell, S. L. (2019). Cardiomyopathy Mutations in Metavinculin Disrupt Regulation of Vinculin-Induced F-Actin Assemblies. *Journal of molecular biology*, *431*(8), 1604–1618.

14. Thompson, P. M., Ramachandran, S., Case, L. B., Tolbert, C. E., Tandon, A., Pershad, M.,Campbell, S. L. (2017). A Structural Model for Vinculin Insertion into PIP2-Containing Membranes and the Effect of Insertion on Vinculin Activation and Localization. Structure, 25(2), 264-275.